

$\pi/K/p$ Identification With a Large-Aperture
Ring-Imaging Cerenkov Counter

M. Adams, A. Bastin, G. Coutrakon, H. Glass, D. Jaffe, J. Kirz and R. McCarthy
SUNY at Stony Brook, Stony Brook, NY 11794

J.R. Hubbard, Ph. Mangeot, J. Mullie, A. Peisert and J. Tichit
CEN Saclay, F91190 Gif-sur-Yvette, France

R. Bouclier, G. Charpak, J.C. Santiard and F. Sauli
CERN, EP Division, 1211 Geneve 23, Switzerland

J. Crittenden, Y. Hsiung and D. Kaplan
Columbia University, Nevis Labs, Box 137, Irvington, NY 10533

C. Brown, S. Childress, D. Finley, A. Ito, A. Jonckheere, H. Jostlein, L. Lederman,
R. Orava, S. Smith, K. Sugano and K. Ueno
FNAL, Box 500, Batavia, IL 60510

A. Maki
KEK, Tsukuba-gun, Ibaraki-ken, 305 Japan

Y. Hemmi, K. Miyake, T. Nakamura, N. Sasao and Y. Sakai
Kyoto University, Kyoto, 606 Japan

R. Gray, R. Plaag, J. Rothberg, J. Rutherford and K. Young
University of Washington, Seattle, WA 98495

ABSTRACT

The operating large aperture ring-imaging Cerenkov detector from FNAL experiment E605 is described. Cerenkov ultraviolet photons are detected with a multi-step avalanche chamber using a He/TEA gas mixture and $\pi/K/p$ separation is obtained from 50 to 200 GeV/c.

INTRODUCTION

We have constructed and operated a large-aperture ring-imaging Cerenkov counter to identify high momentum hadrons in a high intensity experiment at Fermilab (E605). Cerenkov photons were detected by a multi-step avalanche chamber via photoionization of triethylamine (TEA) vapor, yielding approximately three photons for our highest velocity particles. Preliminary analysis of a subset of our data from a spring 1982 test run has obtained $\pi/K/p$ separation up to 200 GeV/c. Over 80% of our particles, having at least one photon, have been unambiguously identified.

Experimental configuration. Figure 1 is a diagram of Fermilab Experiment 605. Our Cerenkov counter is separated from the target by two spectrometer magnets (total kick ~ 6 GeV for this data) which help reduce particle fluxes at our counter. We accept particles over a wide angular range (± 60 mrad vertically). Hadronic trajectories were selected using our calorimeter system and tracked by our chamber system.

Cerenkov Counter Description

Radiator vessel

The design of our Cerenkov counter is based upon a successful prototype¹. We used pure helium as the radiator gas in order to limit chromatic dispersion. The radiator vessel is a thin-walled (.24 cm) aluminum (6061-T6) box. All permanent joints in this structure were welded, taking care to avoid pinholes. Non-permanent joints (at the detector and monitoring ports) were sealed with viton O-rings. Structural strength was provided by aluminum channels and I-beams exterior to the vessel. The side walls were allowed to flex under pressure changes without cracking any welds. The vessel is 15.2 m long and $3.1 \times 2.8 \text{ m}^2$ in cross section at its widest point (near the detectors). The length is sufficient to obtain about 6 detected photons from one particle¹, assuming 100% He transmission, and the cross section was chosen to contain all trajectories of experimental interest.

The vessel has two detector ports, one on each side. For this initial run, only one port was used. The ports are located outside the experimental aperture, so only Cerenkov photons are seen by the detectors.

Our paramount concern in constructing the Cerenkov vessel was that the helium radiator gas should not become contaminated. Since purity better than 1 ppm is required against some contaminants (oxygen), care was taken to eliminate all materials from the vessel other than aluminum, steel, viton, glass, MgF_2 , and CaF_2 . The vessel was cleaned with freon, flushed with nitrogen gas and baked at 100°C for 18 hours before filling with pure helium from liquid boiloff.

The radiator gas was maintained at room temperature and slightly above atmospheric pressure. For typical running conditions, the mean index of refraction was $n^2 - 1 = 73.0 \times 10^{-6}$, giving a threshold $\gamma_t = 118$. This translated into threshold momenta of 16 GeV/c for π 's, 58 GeV/c for K's, and 110 GeV/c for p's.

Gas purification system

The photon transmission of the He gas was maintained by recirculation through a purification system. As the gas enters the purifier, it is mixed with a small amount of hydrogen and put through a Deoxo catalyst (Engelhard Systems, N.J.). The gas then passes through a dryer and a liquid nitrogen cold trap, which extracts and freezes out gas impurities. Gas purity was monitored using a UV light source¹, and the gas transmission was measured to be about 80%, a value somewhat lower than anticipated. Flow rate through the purifier was approximately two volume changes per day.

Mirrors

The full mirror assembly consists of a 4 x 4 array of mirror segments, each a 63.5 X 66 cm² rectangle. For this initial run, only 8 of the mirror segments were available. These segments were placed in the two central columns of our array, subtending an area 132 x 254 cm² (half the aperture). Both mirror columns were focussed onto the right (as seen by an incident proton) detector port.

We used the largest segments available consistent with good reflectivity at 1500 angstroms. Each segment² was ground from a 2.2 cm thick blank of annealed plate glass to a spherical radius of 16.00 ± 0.02 m. The surface was polished to an rms roughness less than 30 angstroms. The figure accuracy of the spherical surface was better than 20 μ rad (error in the normal) over any 18 cm diameter circle: The spherical surfaces were coated with aluminum and MgF₂ to attain a reflectivity of 75% at 1500 angstroms.

The mirrors were hung from above using piano wire. Adjustments in mirror orientation were made from behind, relative to a light aluminum grid. The mass of this grid is mostly located in the mirror gaps in an attempt to keep the mass distribution uniform across the mirror surface. Each mirror segment is held in its own aluminum frame, cushioned by viton.

The mirrors were aligned visually to ± 1 cm accuracy in image position on the detector plane. Our system is self-calibrating using particle tracks with three or more photons. Each mirror was independently aligned so that ring

images from adjacent mirrors were non-overlapping. This was done to minimize confusion in point reconstruction. Mirror alignment angles were chosen so as to minimize the necessary detector area required to see trajectories over the whole aperture.

Calcium fluoride window

The window assembly separating the radiator gas from the detector gas was a 4 x 8 mosaic of CaF_2 crystals, each $10 \times 10 \text{ cm}^2$ in area and 4 mm thick. Each crystal was glued to a stainless steel sleeve which in turn was glued to a heavy brass frame, whose thermal expansion properties were similar to those of the crystals. The frame was maintained at the same voltage as the first grid of the detector to minimize electrostatic instabilities. The transmission of the crystals was typically 70%.

Photon detector

The photon detector was a multi-step proportional chamber with a $40 \times 80 \text{ cm}^2$ active area. Figure 2 shows schematically the CaF_2 window, the conversion, preamplification, and transfer gaps (made of stainless steel grids), the proportional wire chamber, and an external double mylar window. This structure was similar to that of the smaller prototype detector described previously^{1,3}.

Spacers were necessary in the PA gap to maintain uniform gap thickness and thus avoid huge increases in gain in the center of the chamber due to electro-static attraction of the two grids^{3,4}. Three carefully machined fiberglass spacers were used, with mylar guard rings. Gain variations were less than 50%.

The proportional chamber anode plane consisted of 192 vertical 20-micron diameter wires spaced every 2 mm. The cathode wires were oriented at ± 45 degrees with respect to the anodes. Each cathode contained 2×384 50-micron diameter wires spaced every 1 mm. The chamber was operated with He(97%)/TEA(3%) gas mixture at a gain of about 10^7 .

Readout system

The anode and cathode wires were read out every 2 mm into LeCroy 2280-series 12-bit ADC's. The LeCroy ADC system is controlled by a processor module which automatically performs pedestal subtraction and data compression. The processor data was read out via CAMAC into an on-line PDP 11/45 computer. On-line monitoring of the detector was performed via the Fermilab MULTI software package.

Particle Identification Procedure

Pulse height information from the ADC's is used to measure the coordinates of each Cerenkov photon. Cathode pulses are spread over 5-6 ADC channels, and a center-of-gravity method is used to find the pulse-center. Anode pulses generally cover a single wire. The point reconstruction algorithm searches for cathode-cathode-anode triplets, rejecting ghost triplets by requiring approximately equal amplitudes in all three planes.

The particle track is defined by two sets of drift chambers on either end of the Cerenkov vessel (fig. 1), and the momentum is calculated from the particle trajectory. We calculated 3 radii from the momentum, one for each particle type hypothesis, π , K, or p. Then, for each mirror capable of intercepting and reflecting photons from the particle, a ring center is calculated on the detector plane. We then measure the distance between each photon candidate point and each calculated ring center, and try to find a set of radii consistent with one of our particle hypotheses.

Effects of Aberrations

The asymmetric geometry of our apparatus introduces aberrations. Spherical aberrations distort the circular ring image to approximately an elliptical shape. The amount of distortion depends on which mirror reflects the photon as well as the particle trajectory, but can be calculated for each photon and the difference between the major and minor axes is always less than 1.4%.

The long radiator results in a ring image which cannot be focused onto a single plane. Photons are emitted along the entire particle trajectory and the best focus is obtained at the circle of least confusion⁵. The image is also astigmatic: it is out of focus on the major and minor axes of the ellipse and in focus in between.

For the set of mirrors on the same side of the apparatus as the photon detector, the astigmatism is very small and produces a typical uncertainty in radius of $\pm 0.07\%$ rms. The mirrors on the away side generate a larger astigmatism, and their ring images have uncertainties in radii of typically $\pm 0.37\%$ rms.

When the second detector and the full complement of 16 mirrors becomes available, a more symmetrical arrangement of mirrors and detectors will result in reducing the uncertainty due to astigmatism to $\pm 0.07\%$ for all mirrors. Even so, the astigmatism in the current run is tolerable with respect to particle identification.

Chromatic dispersion

Chromatic dispersion arises from the dependence of the helium index of refraction upon photon energy, and generates an rms uncertainty of $\pm 0.7\%$ in the radius. This effect can be reduced by adding about 10% CH_4 to the chamber gas, which absorbs higher energy photons^{1,3}.

Pressure and temperature effects

The index of refraction also depends upon pressure and temperature as $n^2 - 1 \propto p/T$. The temperature at various points within the Cerenkov vessel was measured by thermocouples. We observed a non-uniformity in temperature within the vessel. The observed rms uncertainty in temperature was ± 0.9 K, causing an uncertainty in ring radius of $\pm 0.15\%$. While both pressure and temperature fluctuated over the course of a run, the ratio p/T tended to remain roughly constant, and the drift in radius over the course of a run of several hours duration was on the order of 0.03% .

The sum in quadrature of all the above effects gives an uncertainty of $\pm 0.78\%$ in radius. For a pion having a radius of 68.0 mm, this is an uncertainty of ± 0.53 mm.

Tracking effects

The two other major factors affecting the radius resolution are uncertainties in tracking and the inherent resolution of the multi-step chamber itself. Drift chamber resolution of ± 300 μm and momentum measurement errors will result in a deviation of the predicted ring image center of ± 0.1 mm. Momentum is currently determined with our second spectrometer magnet only with $\Delta p/p = 2\%$ at 60 GeV/c and proportional to momentum. The effect on the ring radii is dependent on momentum and particle type. Just above the Cerenkov threshold for Ks, the 2% momentum rms yields a ± 2.5 mm rms radius error. This does not confuse particle identification because K and π radii are separated by 40 mm. At higher momentum, for example 200 GeV/c, we expect $\Delta p/p$ to be approximately 6% and produce a radius rms of ± 0.69 mm. Both of these tracking errors will be reduced with new survey data and magnetic field values. The multi-step chamber resolution is expected to have an rms of ± 350 μm . Identification of one and two-photon events depends crucially on careful ring center and predicted track center measurements. We have aligned mirrors with ring centers calculated from three-or-more photon events and then improved the survey with photon circles composed from all events.

Momentum measurements are still in a developmental stage and contribute to ring radius errors at high momentum at this time. All results will improve with field maps of both magnets and software improvements in the multi-step chamber resolution of photon clusters.

π/K separation

Looking at the scatter plot of radius vs momentum in figure 5, we see a clear separation of π s and Ks out to 150 GeV/c. A few protons are also observed at the higher momenta. The width of the π peak in the radius distribution of figure 6 is 3.5 mm FWHM and can be reduced when spherical aberrations are accounted for.

The predicted Cerenkov ring centers of all identified particles hitting one of our mirrors are superimposed on figure 7. We see kaons inside a pion ring and observe some change of radius width as a function of the ϕ angle.

Spherical aberrations distort the circular shape of the Cerenkov ring of the detector, but are correctable on a photon by photon basis. This correction improves the single photon π radius resolution from 3.5 mm FWHM to 2.3 mm. This resolution, which allows us to separate π s, Ks and ps up to 200 GeV/c, improves when more than one photon is detected and we are investigating methods of reducing the width even further with careful chamber channel gain balancing.

Particle identification results

Particle identification results of single hadrons for a small percentage of our test run data are summarized in Table 1. The trigger for these events required a calorimeter energy deposit greater than 50 GeV. We have unambiguously identified 82% of the events with at least one photon associated with the track. Multitrack analysis is in a more preliminary stage. Matching tracks with photons from overlapping Cerenkov rings is the major complication for pair events, so currently only single track events have been used for threshold and photon multiplicity studies.

Zero-Photon events

The large number of zero-photon events is consistent with the expected number of kaons and protons near and below threshold. The measured number of photons in K events as a function of momentum agrees with the number expected from the fit of the π 's photon multiplicity Poisson distribution. The contribution of kaons and pions to the zero-photon sample is calculated from the π 's observed mean number of photons. We find that the π^+/K^+ ratio is approximately 2 and constant over momentum. If we identify the zero-photon sample which remains after subtracting the K and π contribution with protons, we find the π^+/p ratio to be approximately 2.5 and also constant over the momentum range 60-130 GeV/c. Both observed particle ratios are in rough agreement with measurements by a previous experiment⁶. We find that above 70 GeV/c zero-photon events can be interpreted as protons with 70% confidence.

Acknowledgments

The authors wish to thank the staffs of Stony Brook, Saclay, CERN, and Fermilab for their technical expertise. This work was supported in part by grants from the National Science Foundation and the Department of Energy.

References

1. G. Coutrakon et. al., IEEE Transactions on Nuclear Science NS-29 (1982) 323.
2. Purchased from Muffoletto Optical Company, 6100 Everall Avenue, Baltimore, MD 21206.
3. R. Bouclier et. al., N.I.M. 205 (1983) 403.
4. J. R. Hubbard et. al., N.I.M. 176 (1980) 293.
5. see, for example, F. Jenkins and H. White, Fundamentals of Optics, McGraw-Hill (1957).
6. H. Jostlein et. al., Phy. Rev. D20 (1979) 53.

Total number of events in sample = 20584

Particles identified by at least one photon:

π^+ = 8383 π^- = 1374 total π = 9757

K^+ = 2267 K^- = 110 total K = 2377

p = 65 \bar{p} = 6 total p, \bar{p} = 71

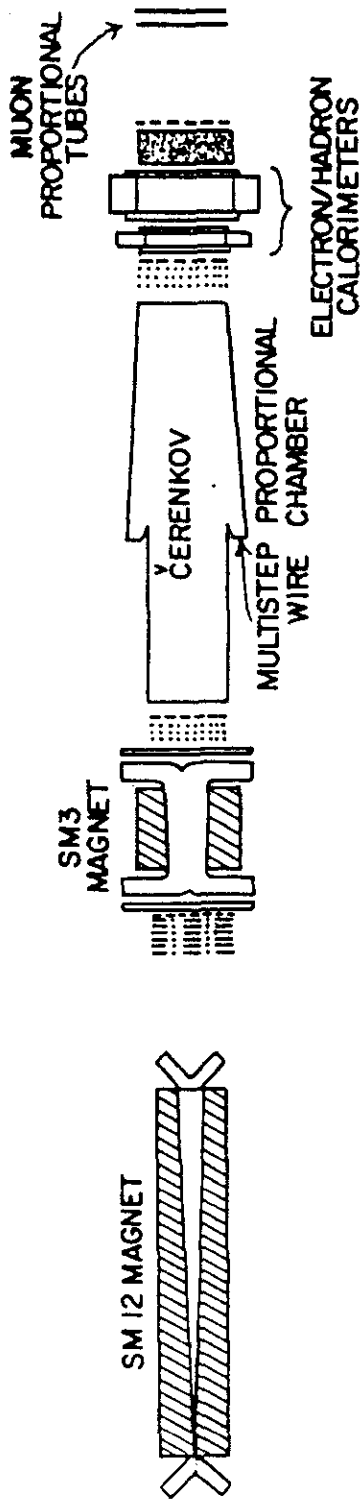
Ambiguous events = 2877

Zero-photon events = 5502

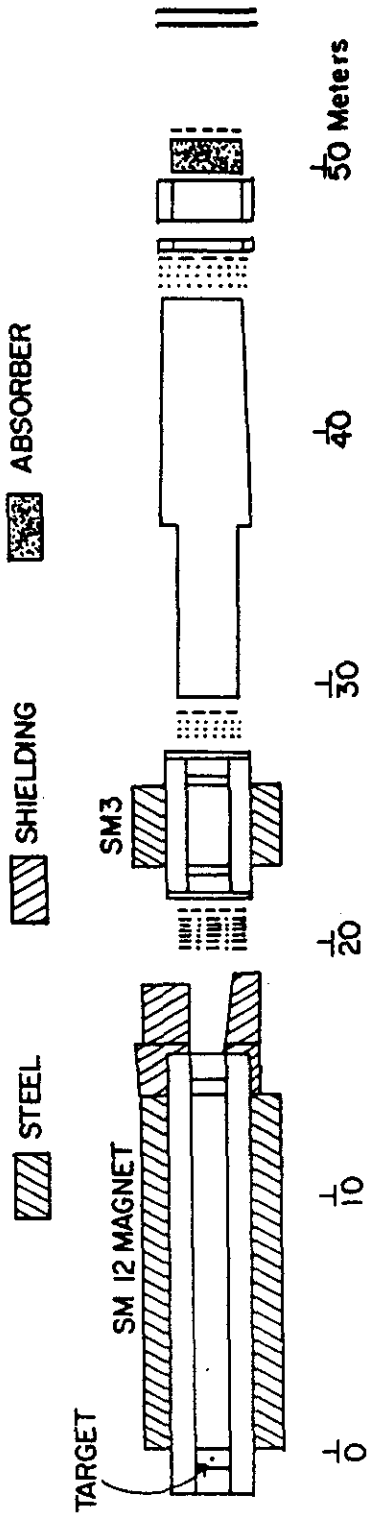
Table I. Summary of preliminary particle identification results for single-track hadron events

Figure Captions

- Figure 1. Experiment E-605
- Figure 2. The multi-step avalanche chamber, showing spacing between planes and typical operating voltages.
- Figure 3. An off-line display of a 5-photon π event. Cathode pulses are inclined at 45° in the left and right margins, anode pulse heights are shown at the top. The reconstructed photon positions are indicated by *, and the predicted ring center by + and mirror label.
- Figure 4. Distribution of the number of photons for π s. A Poisson distribution with a mean of 2.7 is superimposed. For this fit, $\chi^2 = 11$ for 8 degrees of freedom.
- Figure 5. Scatter plot of radius vs momentum for events having at least two photons. Curves showing the expected radii for π , K and p are superimposed.
- Figure 6. Radius distribution for all photons with events in the momentum band $80 < p < 100$ GeV/c.
- Figure 7. Radius of photons from the track-predicted ring center vs. ϕ angle in the detector plane.



PLAN VIEW E 605



ELEVATION SECTION E605

- DRIFT CHAMBER
- - - - - PROPORTIONAL CHAMBER
- COUNTER BANK

